LETTER

doi:10.1038/nature11149

Programmable single-cell mammalian biocomputers

Simon Ausländer[1], David Ausländer[1], Marius Müller[1], Markus Wieland[1] & Martin Fussenegger[1,2]

Synthetic biology has advanced the design of standardized control devices that program cellular functions and metabolic activities in living organisms[1]. Rational interconnection of these synthetic switches resulted in increasingly complex designer networks that execute input-triggered genetic instructions with precision, robustness and computational logic reminiscent of electronic circuits[2,3]. Using trigger-controlled transcription factors, which independently control gene expression[4,5], and RNA-binding proteins that inhibit the translation of transcripts harbouring specific RNA target motifs[6,7], we have designed a set of synthetic transcription–translation control devices that could be rewired in a plug-and-play manner. Here we show that these combinatorial circuits integrated a two-molecule input and performed digital computations with NOT, AND, NAND and N-IMPLY expression logic in single mammalian cells. Functional interconnection of two N-IMPLY variants resulted in bitwise intracellular XOR operations, and a combinatorial arrangement of three logic gates enabled independent cells to perform programmable half-subtractor and half-adder calculations. Individual mammalian cells capable of executing basic molecular arithmetic functions isolated or coordinated to metabolic activities in a predictable, precise and robust manner may provide new treatment strategies and bio-electronic interfaces in future gene-based and cell-based therapies.

Today's electronic devices are controlled by binary calculations executed by electrons flowing through metal wires that are interconnected as multi-layered logic gates. Similarly, natural and synthetic gene circuits can be encoded and chemically rewired to integrate environmental and cellular signals and perform logic metabolic computations controlling physiological activities[2,3,8–10]. With its defining modular design and standardization principles[1], synthetic biology has significantly advanced the construction of genetic circuit components that control transcription or translation in a trigger-inducible manner[11–13]. The standardized and modular design of these gene switches improved compatibility for the 'plug-and-play' construction of higher-order networks that function in bacterial, yeast and mammalian cells after minor refinements[12]. Examples of synthetic networks with similar circuit topology in different species include logic gates[2,3,9,14,15], molecular counters[8], molecular timing devices[16], synthetic eco-sensing and quorum-sensing/hormone systems[17,18], band-pass filters[19,20] and different types of oscillator that program rhythmic transgene expression with tunable frequency and amplitude[21,22].

Many of the transcription-control devices used share a common two-component design: a synthetic transcription factor containing a trigger-controlled DNA-binding motif fused to a transactivation domain binds to a specific operator, thereby activating adjacent minimal promoters in an adjustable manner[12]. For example, the antibiotic erythromycin fine-tunes the induction of the synthetic promoter P_{ETR2} by the erythromycin-dependent transactivator (ET1)[5], and the apple metabolite phloretin modulates the activation of the chimeric promoter P_{TtgR1} by the phloretin-dependent transactivator ($TtgA_1$)[4] (Fig. 1). RNA controllers are proteins or nucleic acids that vary translation when binding to complementary natural or synthetic RNA motifs engineered into transcripts[6,7,23]. For example, the bacteriophage MS2 coat protein (MS2) binds to the MS2box RNA motif ($MS2_{box}$)[6], and the archaeal ribosomal protein L7Ae interacts with its cognate C/Dbox RNA structure (C/D_{box})[7,24] (Fig. 1). These transcription- and translation-control components were wired into the following genetic switchboard: input molecules (erythromycin or phloretin) abolish the binding of the transcription factors (ET1 or $TtgA_1$), which otherwise transactivate their cognate promoters (P_{ETR2} or P_{TtgR1}) and drive expression of the RNA-binding protein (MS2 or L7Ae) or a transcript encoding the protein-specific RNA box ($MS2_{box}$ or C/D_{box}) and the destabilized fluorescent reporter gene (encoding d2EYFP or dsRed) (Fig. 1). Both transcription units are functionally connected by the RNA-binding proteins (MS2 or L7Ae) which inhibit the translation of transcripts containing the cognate RNA boxes ($MS2_{box}$ or C/D_{box}) (Fig. 1). Combinatorial assembly and permutation of the controller components in this genetic switchboard enabled the design of distinct computational circuits containing up to six different expression units and performing specific digital logic operations. Each of the Boolean circuits integrates a two-molecule input into a digital ON/OFF expression decision, following the processing logic of NOT, NAND and N-IMPLY gates (Fig. 2; see Supplementary Fig. 1 for control experiments showing component leakiness and threshold-defining settings for fluorescence-activated cell sorting (FACS)). The N-IMPLY circuits, which are exclusively induced in the presence of only one specific input molecule, were wired in two different formats. The first was an A ANDNOT B circuitry, in which the translation of a phloretin-controlled $TtgA_1$-mediated P_{TtgR1}-driven d2EYFP transcript containing a C/Dbox in its 5′ untranslated region (5′ UTR) could be inhibited by erythromycin-controlled ET1-mediated P_{ETR2}-driven expression of the C/Dbox-binding protein L7Ae (Fig. 2a). The second format was a

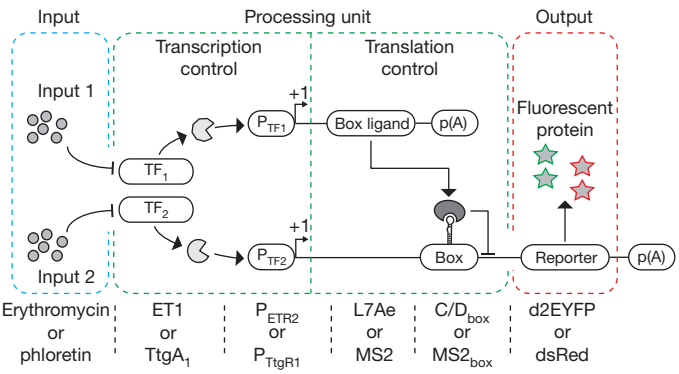

Figure 1 | Genetic switchboard of the biocomputer circuitry. Two input molecules (inputs 1 and 2) inactivate transcription factors (TF_1 and TF_2), which otherwise induce promoters (P_{TF1} and P_{TF2}) that drive the transcription of expression units either encoding an RNA-binding protein (box ligand) or containing an RNA target unit in the 5′ UTR (box) and a reporter gene. Both expression units are interconnected through the box ligand, whose interaction with its target box inhibits reporter gene translation. Sequential wiring of the input module (blue) to the processing unit providing bitwise integrations of transcription and translation control activities (green) produces a digital output (red). See Supplementary Information for extended figure legends.

[1]Department of Biosystems Science and Engineering, Eidgenössische Technische Hochschule Zürich, Mattenstrasse 26, CH-4058 Basel, Switzerland. [2]Faculty of Science, University of Basel, Mattenstrasse 26, CH-4058 Basel, Switzerland.

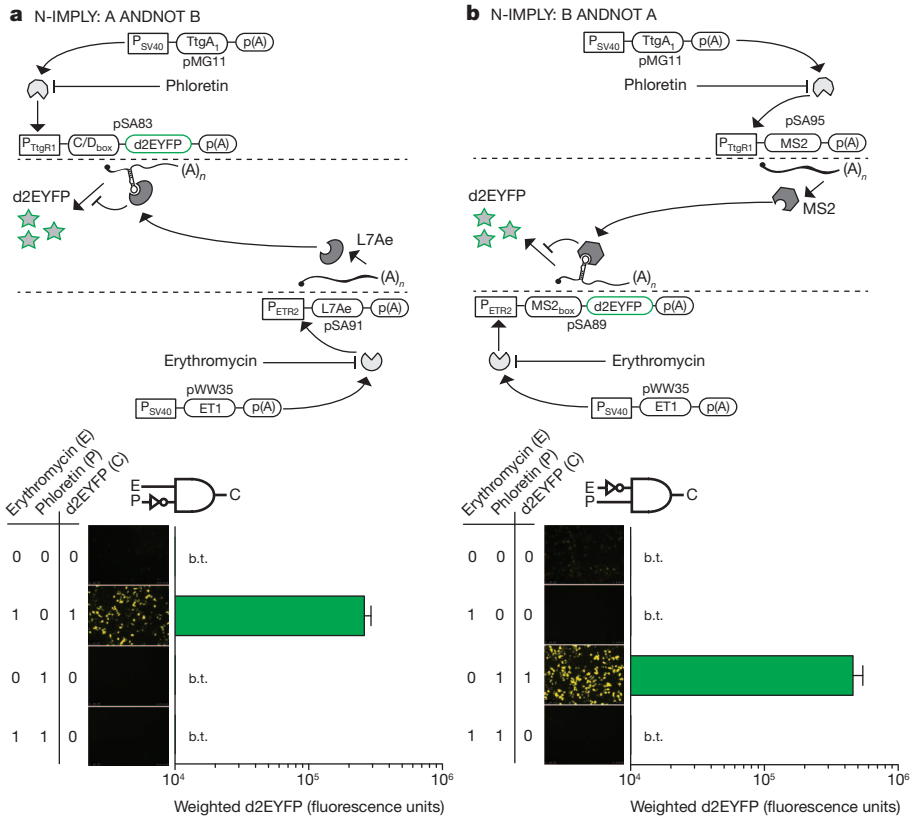

Figure 2 | Design and processing performance of synthetic N-IMPLY gates in human cells. a, A ANDNOT B logic gate. By combining the two input signals erythromycin and phloretin in accordance with the truth table, transfected HEK-293 cells are programmed to produce d2EYFP exclusively in the presence of erythromycin and not phloretin as shown by fluorescence microscopy and FACS analysis. **b**, B ANDNOT A logic gate. By combining the two input signals erythromycin and phloretin in accordance with the truth table, transfected HEK-293 cells are programmed to produce d2EYFP exclusively in the presence of phloretin and not erythromycin as shown by fluorescence microscopy and FACS analysis. b.t., below the threshold of 10^4 fluorescence units. Error bars represent s.d.; n = 3.

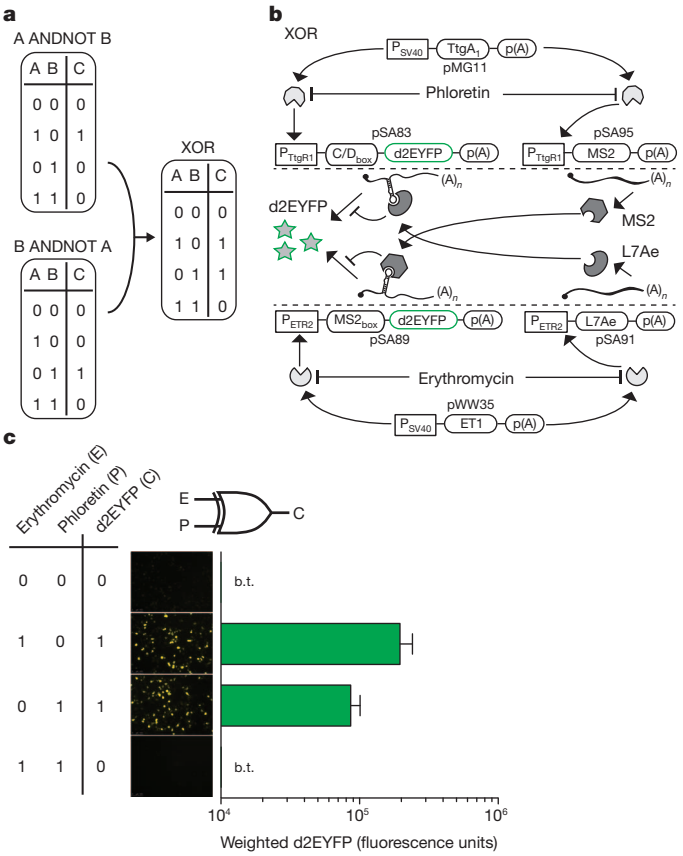

Figure 3 | Design and computation characteristics of the synthetic mammalian XOR processor. a, Truth tables illustrating how the combination of two different N-IMPLY gates results in XOR processing, characterized by switching the output ON if exactly one of the input signals is present. **b**, Genetic switchboard of the XOR circuitry (see Supplementary Information for functional description). **c**, By combining the two input signals in accordance with the truth table, transfected HEK-293 cells are programmed to produce d2EYFP, following XOR computation logic: reporter gene expression is switched ON exclusively in the presence of either erythromycin or phloretin as shown by fluorescence microscopy and FACS analysis. Error bars represent s.d.; n = 3.

B ANDNOT A circuitry, in which an erythromycin-controlled ET1-mediated P_{ETR2}-driven d2EYFP transcript containing a MS2box in its 5′ UTR could be inhibited by phloretin-controlled P_{TtgR1}-driven expression of the MS2 protein (Fig. 2b). After simultaneous transfection of the system-encoding vectors into human embryonic kidney cells (HEK-293), fluorescent reporter gene expression was digitally controlled and exclusively induced when either erythromycin (A ANDNOT B) or phloretin (B ANDNOT A) was present (Fig. 2a, b). As indicated by the consistency of fluorescence microscopy and FACS-mediated single-cell analysis, the cellular N-IMPLY computations executed by the interconnected transcription/translation controllers were remarkably robust (Fig. 2a, b). Detailed control experiments confirmed that the inducer molecules did not influence cell viability[4,5] and showed that they had no effect on constitutive d2EYFP or dsRed expression levels at repressing concentrations (Supplementary Fig. 2a, b). Furthermore, there was no relevant interference between the RNA-controlling modules, which ensures high specificity of the engineered N-IMPLY gates (Supplementary Fig. 3a, b).

To test whether the transcription/translation-control devices could also be interconnected in a predictable manner to higher-order designer

networks with complex computation logic we chose to engineer the XOR gate. XOR computations are particularly challenging to design because they integrate two different input signals and produce the output ON exclusively if one of the inputs is ON (Fig. 3a). Because of this complexity, XORs have so far only been constructed in non-cellular deoxyribozyme-based circuits[25] and as intercellular crosstalk in bacteria[3] and yeast[2]. Engineering HEK-293 cells with all components of both N-IMPLY gates (A ANDNOT B as well as B ANDNOT A) encoded on six different plasmids human cells produced d2EYFP with digital XOR expression logic after the addition of different combinations of the trigger-molecules erythromycin and phloretin (Fig. 3b, c). Although both d2EYFP expression units are completely transactivated by their respective transcription factors in the absence of input signals, the RNA controllers were able to inhibit translation efficiently and prevent d2EYFP expression (Fig. 3c). As required, the output of the XOR gate was also repressed in the presence of both input signals when both transcription factors were inactivated and also when neither of the two d2EYFP expression units was expressed. However, addition of either erythromycin or phloretin resulted in inactivation of the corresponding transcription factor, whereas its counterpart remained active and induced its respective d2EYFP expression unit (Fig. 3c). For rigorous analysis of network dynamics and the contribution of individual system components to the computation behaviour we decomposed the XOR circuit by sequentially removing individual components; this resulted in distinct circuits that performed specific logic computations (Supplementary Fig. 4). Taking away either of the reporter genes resulted in N-IMPLY gates (Supplementary Fig. 4a, b), elimination of either transcription factor generated two distinct NOT gates (Supplementary Fig. 4c, d), and removal of either translation inhibitor produced two different gates with NAND logic (Supplementary Fig. 4e, f). These results underline the rational and predictable plug-and-play characteristic of the transcription/translation-control components and show that these individual components can be readily rewired into combinatorial structures to perform biocomputing activities ranging from simple NOT gates to complex XOR gates.

As a next step towards programmable single-cell biocomputers we added another layer of computation capacity to the XOR gate to design a half-subtractor, which is commonly used in digital electronics as a

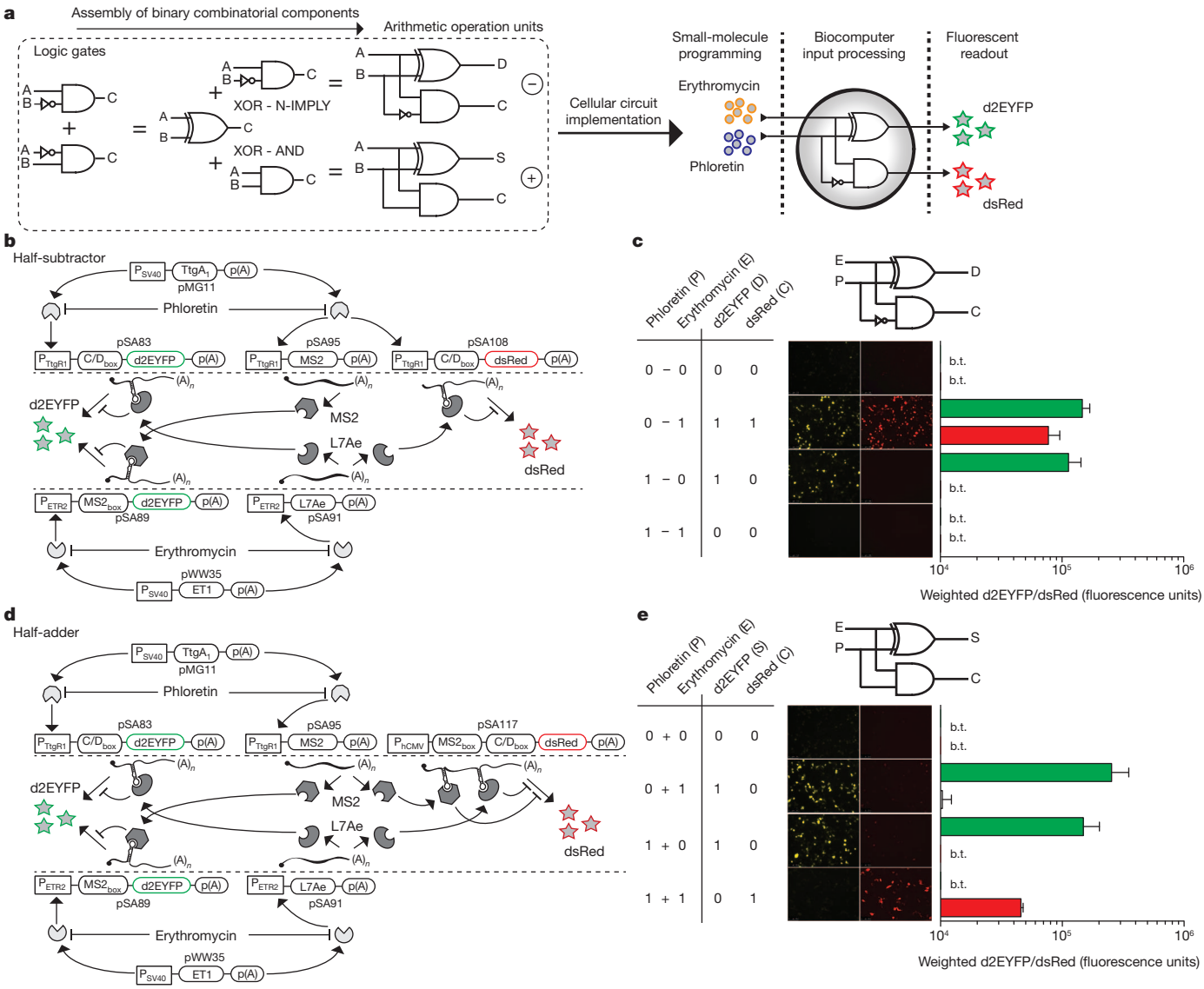

Figure 4 | Input-programmable half-subtractor and half-adder operations. **a**, Electronic circuit diagram illustrating the design of biocomputer circuits by combinatorial assembly of logic gates. **b**, Genetic switchboard of the programmable single-cell half-subtractor. **c**, Fluorescence micrographs and single-cell FACS analysis of the half-subtractor performing arithmetic subtraction of the erythromycin input from the phloretin input by calculating the difference D (d2EYFP) and borrow C (dsRed). **d**, Genetic switchboard of the programmable single-cell half-adder. **e**, Fluorescence micrographs and single-cell FACS analysis of the half-adder performing arithmetic addition of the erythromycin input and the phloretin input by calculating the sum S (d2EYFP) and carry C (dsRed). Error bars represent s.d.; n = 3.

binary arithmetic circuit capable of performing a subtraction of two bits. The half-subtractor was designed by combination of the XOR gate, which calculates the difference D, and an N-IMPLY gate to calculate the borrow C (Fig. 4a). The additional N-IMPLY gate (A ANDNOT B) was constructed by replacing the yellow fluorescent reporter gene of the aforementioned A ANDNOT B gate with dsRed so that its modified phloretin-regulated and L7Ae-controlled reporter unit would produce a red fluorescent output (Supplementary Fig. 5a). When placing this seven-component multi-processing device into human cells it performed precise two-input–two-output integration, showing half-subtractor calculation characteristics as predicted (Fig. 4b, c). Despite its high complexity, the half-subtractor performance was robust as indicated by the correlation of fluorescence microscopy and FACS analysis (Fig. 4c). In addition, in the presence of erythromycin, which programmed the half-subtractor to express both reporter genes, yellow and red fluorescence micrographs show almost perfect correlation, which suggests that the observed processing behaviour did indeed result from single-cell computations (Fig. 4c).

Besides the half-subtractor, the half-adder, which calculates the addition of two bits, is the second (bio)computer unit providing fundamental arithmetic operations. Together they manage any calculation in digital electronics. The design of a genetically encoded half-adder requires the combination of an XOR gate and an AND gate (Fig. 4a). The AND gate consists of a dsRed expression unit whose transcripts contain both MS2box and C/Dbox RNA motifs in their 5′ UTR. They block the translation of dsRed on binding to MS2 or L7Ae, respectively. When MS2 transcription is set for repression by phloretin and L7Ae production is controlled in an erythromycin-repressible manner, pSA117-encoded dsRed is only expressed in the presence of both phloretin and erythromycin (Supplementary Fig. 5c). The pSA117-derived control vector lacking any RNA motifs showed constitutive dsRed expression (Supplementary Fig. 5d). Combination of this AND gate, which determines the carry C, with the aforementioned XOR gate (Fig. 3) calculating the sum S resulted in robust half-adder-specific computations in individual cells that can be programmed by a distinct set of input signals (Fig. 4d, e). Quantitative fluorescence profiling of entire circuit-transfected populations using a plate reader showed mean induction factors (OFF/ON) of 12 (d2EYFP) and 13 (dsRed) for the half-subtractor (Supplementary Figs 6a and 7a) and 14 (d2EYFP) and 4 (dsRed) for the half-adder (Supplementary Figs 6b and 7b). Furthermore, time-lapse fluorescence microscopy of entire circuit-transfected populations confirmed half-subtractor and half-adder processing dynamics in real time (Supplementary Movies 1 and 2).

In digital electronics the presence or absence of electrons represents the unique input signals, which allows multi-bit processing in a switchboard of multi-layered logic gates performing distinct calculations. The flow of electrons through the switchboard can be programmed to process desired algorithms. Although the design of electronic computers has achieved enormous processing power, living mammalian cells are in principle no less powerful, because they constantly process logic operations and perform countless physiological computations in parallel to coordinate endogenous metabolites and interface with environmental signals[26]. Single-cell biocomputers are therefore compatible with any physiological trigger input that increases parallel processing power; they may be genetically programmed to execute encoded activities; they are scalable to tissue structures; and they are straightforward to interface with host metabolism to achieve therapeutic impact. Examples of synthetic biocomputing devices that sense signal input and process a coordinated therapeutic output such as sophisticated cancer kill switches integrating multi-input transformation signals[10,11,27] were first tested in cell cultures, but pioneering one-input widgets such as T-cell population controllers[28], artificial insemination devices[29], blue-light-triggered glucose homeostasis for diabetes therapy[13] and prosthetic gouty arthritis networks for the treatment of hyperuricemic disorders[30] have been used successfully to perform therapeutic calculations when implanted and plugged into the metabolism of animals.

Programming single mammalian cells to perform multi-bit processing has been extremely challenging because the computations must operate in functional isolation from the cellular metabolism. Complex multi-bit processing devices have therefore been engineered in which individual processing components are encoded in single bacterial[3] or yeast[2] cells, which communicate through chemical wires to perform computations in multicellular assemblies. We have successfully merged transcription and translation controllers in a combinatorial plug-and-play manner to achieve synthetic networks ranging from simple logic gates to complex XOR controllers as well as half-subtractors and half-adders executing fundamental arithmetic operations. Mammalian cells engineered with programmable genetic devices performing arithmetic calculations with similar precision, robustness and predictability to those of their digital electronics counterparts may enable the assembly of tissue-like biocomputers that could allow the design of complex human–machine interfaces and provide diagnostic information and therapeutic interventions in future gene-based and cell-based treatment strategies.

METHODS SUMMARY

Biocomputer design. Construction details for expression vectors are provided in Supplementary Information and Supplementary Table 1. HEK-293T cells (American Type Culture Collection, CRL-11268) were cultivated at 37 °C in DMEM medium (Invitrogen) supplemented with 10% FCS (lot no. PE01026P; Bioconcept) and 1% penicillin/streptomycin solution (Sigma-Aldrich) in a humidified atmosphere containing 5% CO_2. HEK-293 cells were (co)-transfected with biocomputer-encoding plasmids (Supplementary Table 2) by using a polyethyleneimine-based protocol. At 6 h after transfection, the cells were re-seeded into 96-well plates containing erythromycin (2.7 μM; stock solution: 5 mg ml^{-1} in 100% ethanol; Sigma Aldrich) and phloretin (50 μM; stock solution: 14.5 mM in 100% ethanol; Sigma Aldrich) as indicated and cultivated for a further 62 h before analysis (Supplementary Fig. 8).

Flow cytometry. Cell populations were analysed with a LSRII Fortessa flow cytometer (Becton Dickinson) equipped for d2EYFP (488-nm laser, 505-nm longpass filter and 530/30 emission filter (passband centred on 530 nm; passband width 30 nm)) and dsRed (561 nm laser, 505-nm longpass filter and 586/15 emission filter) detection and set to exclude dead cells and cell doublets. Each sample was spiked with AlignFlow alignment beads (A-7302; Life Technologies) as internal control, ensuring consistency of flow cytometry settings among different circuits and independent experiments (Supplementary Fig. 9). At least 10,000 cells were recorded per data set and analysed with FACSDiva (version no. 6.1.3; BD Biosciences). To score digital expression profiles of the biocomputer devices, transfected HEK-293 populations were gated for cells with high d2EYFP/yellow or dsRed/red expression/fluorescence levels beyond a threshold of 10^4 arbitrary fluorescence units (see Supplementary Fig. 1 for control and FACS threshold-defining experiments and Supplementary Fig. 10 for raw data on circuit performance). The percentage of gated cells was multiplied by their median fluorescence, resulting in a weighted d2EYFP/dsRed expression value that correlated fluorescence intensity with cell number.

Full Methods and any associated references are available in the online version of the paper at www.nature.com/nature.

Received 4 November 2011; accepted 17 April 2012.
Published online 3 June 2012.

1. Khalil, A. S. & Collins, J. J. Synthetic biology: applications come of age. *Nature Rev. Genet.* **11,** 367–379 (2010).
2. Regot, S. *et al.* Distributed biological computation with multicellular engineered networks. *Nature* **469,** 207–211 (2011).
3. Tamsir, A., Tabor, J. J. & Voigt, C. A. Robust multicellular computing using genetically encoded NOR gates and chemical 'wires'. *Nature* **469,** 212–215 (2011).
4. Gitzinger, M., Kemmer, C., El-Baba, M. D., Weber, W. & Fussenegger, M. Controlling transgene expression in subcutaneous implants using a skin lotion containing the apple metabolite phloretin. *Proc. Natl Acad. Sci. USA* **106,** 10638–10643 (2009).
5. Weber, W. *et al.* Macrolide-based transgene control in mammalian cells and mice. *Nature Biotechnol.* **20,** 901–907 (2002).
6. Paraskeva, E., Atzberger, A. & Hentze, M. W. A translational repression assay procedure (TRAP) for RNA–protein interactions *in vivo*. *Proc. Natl Acad. Sci. USA* **95,** 951–956 (1998).
7. Saito, H., Fujita, Y., Kashida, S., Hayashi, K. & Inoue, T. Synthetic human cell fate regulation by protein-driven RNA switches. *Nature Commun.* **2,** 160 (2011).

8. Friedland, A. E. *et al.* Synthetic gene networks that count. *Science* **324,** 1199–1202 (2009).
9. Leisner, M., Bleris, L., Lohmueller, J., Xie, Z. & Benenson, Y. Rationally designed logic integration of regulatory signals in mammalian cells. *Nature Nanotechnol.* **5,** 666–670 (2010).
10. Xie, Z., Wroblewska, L., Prochazka, L., Weiss, R. & Benenson, Y. Multi-input RNAi-based logic circuit for identification of specific cancer cells. *Science* **333,** 1307–1311 (2011).
11. Culler, S. J., Hoff, K. G. & Smolke, C. D. Reprogramming cellular behavior with RNA controllers responsive to endogenous proteins. *Science* **330,** 1251–1255 (2010).
12. Weber, W. & Fussenegger, M. Molecular diversity–the toolbox for synthetic gene switches and networks. *Curr. Opin. Chem. Biol.* **15,** 414–420 (2011).
13. Ye, H., Daoud-El Baba, M., Peng, R. W. & Fussenegger, M. A synthetic optogenetic transcription device enhances blood-glucose homeostasis in mice. *Science* **332,** 1565–1568 (2011).
14. Kramer, B. P., Fischer, C. & Fussenegger, M. BioLogic gates enable logical transcription control in mammalian cells. *Biotechnol. Bioeng.* **87,** 478–484 (2004).
15. Win, M. N. & Smolke, C. D. Higher-order cellular information processing with synthetic RNA devices. *Science* **322,** 456–460 (2008).
16. Weber, W. *et al.* A synthetic time-delay circuit in mammalian cells and mice. *Proc. Natl Acad. Sci. USA* **104,** 2643–2648 (2007).
17. Weber, W., Daoud-El Baba, M. & Fussenegger, M. Synthetic ecosystems based on airborne inter- and intrakingdom communication. *Proc. Natl Acad. Sci. USA* **104,** 10435–10440 (2007).
18. You, L., Cox, R. S. III, Weiss, R. & Arnold, F. H. Programmed population control by cell–cell communication and regulated killing. *Nature* **428,** 868–871 (2004).
19. Basu, S., Gerchman, Y., Collins, C. H., Arnold, F. H. & Weiss, R. A synthetic multicellular system for programmed pattern formation. *Nature* **434,** 1130–1134 (2005).
20. Greber, D. & Fussenegger, M. An engineered mammalian band-pass network. *Nucleic Acids Res.* **38,** e174 (2010).
21. Danino, T., Mondragon-Palomino, O., Tsimring, L. & Hasty, J. A synchronized quorum of genetic clocks. *Nature* **463,** 326–330 (2010).
22. Tigges, M., Marquez-Lago, T. T., Stelling, J. & Fussenegger, M. A tunable synthetic mammalian oscillator. *Nature* **457,** 309–312 (2009).
23. Ellington, A. D. & Szostak, J. W. *In vitro* selection of RNA molecules that bind specific ligands. *Nature* **346,** 818–822 (1990).
24. Saito, H. *et al.* Synthetic translational regulation by an L7Ae-kink-turn RNP switch. *Nature Chem. Biol.* **6,** 71–78 (2010).
25. Stojanovic, M. N. & Stefanovic, D. Deoxyribozyme-based half-adder. *J. Am. Chem. Soc.* **125,** 6673–6676 (2003).
26. Bandyopadhyay, S. *et al.* Rewiring of genetic networks in response to DNA damage. *Science* **330,** 1385–1389 (2010).
27. Nissim, L. & Bar-Ziv, R. H. A tunable dual-promoter integrator for targeting of cancer cells. *Mol. Syst. Biol.* **6,** 444 (2010).
28. Chen, Y. Y., Jensen, M. C. & Smolke, C. D. Genetic control of mammalian T-cell proliferation with synthetic RNA regulatory systems. *Proc. Natl Acad. Sci. USA* **107,** 8531–8536 (2010).
29. Kemmer, C. *et al.* A designer network coordinating bovine artificial insemination by ovulation-triggered release of implanted sperms. *J. Control. Release* **150,** 23–29 (2011).
30. Kemmer, C. *et al.* Self-sufficient control of urate homeostasis in mice by a synthetic circuit. *Nature Biotechnol.* **28,** 355–360 (2010).

Supplementary Information is linked to the online version of the paper at www.nature.com/nature.

Acknowledgements We thank R. Singer for providing pMS2dIFG, M. Tigges for generous advice, E. Gutzwiller for experimental support, and M. Dessing and V. Jäggin for assistance with flow cytometry. This work was supported by the Swiss National Science Foundation (grant no. 31003A-126022) and in part by EC Framework 7 (Persist).

Author Contributions S.A., D.A., M.M., M.W. and M.F. designed the project, analysed results and wrote the manuscript. S.A., D.A. and M.M. performed the experimental work.

Author Information Reprints and permissions information is available at www.nature.com/reprints. The authors declare no competing financial interests. Readers are welcome to comment on the online version of this article at www.nature.com/nature. Correspondence and requests for materials should be addressed to M.F. (fussenegger@bsse.ethz.ch).

METHODS

Biocomputer components. Comprehensive design and construction details for all expression vectors are provided in Supplementary Table 1. Key plasmids include the following. pWW35 (ref. 5) encodes constitutive expression of the macrolide-dependent transactivator (ET1; P_{SV40}-ET1-pA). pMG11 (ref. 4) harbours a constitutive expression unit encoding the phloretin-dependent transactivator ($TtgA_1$; P_{SV40}-$TtgA_1$-pA). pSA83 encodes a phloretin-responsive $TtgA_1$-triggered P_{TtgR1}-driven d2EYFP expression unit harbouring a C/Dbox in the 5′ UTR that is targeted by the translation suppressor protein $L7Ae^{24}$ (P_{TtgR1}-C/D_{box}-d2EYFP-pA; GenBank ID JQ624673). pSA89 encodes an erythromycin-responsive ET1-triggered P_{ETR2}-driven d2EYFP expression unit harbouring a MS2box in the 5′ UTR that is targeted by the translation suppressor protein MS2 (ref. 6) (P_{ETR2}-$MS2_{box}$-d2EYFP-pA; GenBank ID JQ624674). pSA91 encodes an erythromycin-responsive ET1-triggered P_{ETR2}-driven L7Ae expression unit (P_{ETR2}-L7Ae-pA; GenBank ID JQ624675). pSA95 encodes a phloretin-responsive $TtgA_1$-triggered MS2 expression unit (P_{TtgR1}-MS2-pA; GenBank ID JQ624676). pSA108 encodes a phloretin-responsive $TtgA_1$-triggered P_{TtgR1}-driven dsRed expression unit harbouring a C/Dbox in the 5′ UTR that is targeted by the translation suppressor protein $L7Ae^{24}$ (P_{TtgR1}-C/D_{box}-dsRed-pA). pSA117 encodes a constitutive P_{hCMV}-driven dsRed expression unit harbouring both MS2box and C/Dbox RNA motifs in its 5′ UTR that are targeted by the translation suppressor proteins MS2 (ref. 6) and $L7Ae^{24}$, respectively (P_{hCMV}-$MS2_{box}$-C/D_{box}-dsRed-pA). The plasmid composition of each circuit is provided in Supplementary Table 2.

Cell culture, transfection and gene regulation. HEK-293T cells (American Type Culture Collection, CRL-11268) were cultivated at 37 °C in DMEM medium (Invitrogen) supplemented with 10% FCS (lot no. PE01026P; Bioconcept) and 1% penicillin/streptomycin solution (Sigma-Aldrich) in a humidified atmosphere containing 5% CO_2. HEK-293 cells were (co)-transfected using an optimized polyethyleneimine-based protocol. In brief, a transfection solution containing 4 μg of plasmid DNA mixtures, 800 μl of FCS-free DMEM and 12 μl of polyethyleneimine (1 mg ml^{-1} in water; Polysciences) was incubated for 30 min at 22 °C before it was added dropwise to 4×10^5 HEK-293 cells seeded in each well of a six-well plate 14 h before transfection (see Supplementary Table 2 for a detailed composition of plasmid DNA mixtures). At 6 h after transfection, the cells were detached for 1 min using 200 μl of trypsin/EDTA (Biowest), washed once in 1 ml of FCS-containing DMEM, resuspended in 0.75 ml of FCS-containing DMEM, re-seeded into 12 wells of a 96-well plate containing the trigger molecules erythromycin (2.7 μM; stock solution: 5 mg ml^{-1} in 100% ethanol; Sigma Aldrich) and phloretin (50 μM; stock solution: 14.5 mM in 100% ethanol; Sigma Aldrich) as indicated and cultivated for a further 62 h before analysis (Supplementary Fig. 8).

Fluorescence imaging. Fluorescence and time-lapse microscopy was performed with an inverted fluorescence microscope (DMI 6000B; Leica Microsystems) equipped with an incubation chamber, a DFC350FX R2 digital camera (Leica), a 10× objective (objective HC PL FL 10×/0.30 PH1 –/D 11.0; Leica), a 495/535-nm (d2EYFP) and 580/630-nm (dsRed) excitation/emission filter set and LAS AF imaging software (FW4000-TZ; Leica). Identical settings including exposure times of 1 s for d2EYFP and dsRed were used for all fluorescence micrographs.

Flow cytometry. All engineered cell populations were analysed with a Becton Dickinson LSRII Fortessa flow cytometer equipped for d2EYFP (488 nm laser, 505 nm longpass filter, 530/30 emission filter (passband centred on 530 nm; passband width 30 nm)) and dsRed (561 nm laser, 505 longpass filter and 586/15 emission filter) detection and set to exclude dead cells and cell doublets. Before analysis, each sample was spiked with AlignFlow alignment beads (A-7302; Life Technologies), serving as an internal control and ensuring consistency of flow cytometry settings between different circuits and independent experiments (Supplementary Fig. 9). At least 10,000 cells were recorded in each data set and analysed with BD FACSDiva (version no. 6.1.3; BD Biosciences). To score digital expression profiles of the biocomputer devices, transfected HEK-293 cell populations were gated for cells with high d2EYFP/yellow or dsRed/red expression/fluorescence levels beyond a threshold of 10^4 arbitrary fluorescence units (see Supplementary Fig. 1 for control and FACS threshold-defining experiments and Supplementary Fig. 10 for raw data on circuit performance). The percentage of gated cells was multiplied by their median fluorescence, resulting in a weighted d2EYFP/dsRed expression value that correlated fluorescence intensity with cell number.

Plate-reader-based fluorescence analysis. Fluorescence of entire circuit-transfected cell populations was profiled with a monochromatic Tecan Infinite 200pro plate reader with excitation and emission set to 488/9 nm and 535/20 nm for d2EYFP, and 560/9 nm and 595/20 nm for dsRed, respectively. Autofluorescence of mock-transfected cells was deducted from circuit-derived fluorescence.